Determination and analysis of time series of CFC-11 (CCl3F) from FTIR solar spectra, in situ observations, and model data in the past 20 years

Environmental Science: Atmospheres

ROYAL SOCIETY OF CHEMISTRY

PAPER

View Article Online
View Journal | View Issue

Cite this: *Environ. Sci.: Atmos.*, 2022, **2**, 1487

Determination and analysis of time series of CFC-11 (CCl_3F) from FTIR solar spectra, *in situ* observations, and model data in the past 20 years above Jungfraujoch (46°N), Lauder (45°S), and Cape Grim (40°S) stations

Irene Pardo Cantos, *[a] Emmanuel Mahieu, [a] Martyn P. Chipperfield,[bc] Dan Smale,[d] James W. Hannigan,[e] Marina Friedrich,[f] Paul Fraser,[g] Paul Krummel, [g] Maxime Prignon, [ah] Jamal Makkor,[i] Christian Servais[j] and John Robinson[d]

Received 31st May 2022
Accepted 22nd September 2022

DOI: 10.1039/d2ea00060a

rsc.li/esatmospheres

The atmospheric concentration of CFC-11 (CCl_3F) has declined in response to the phase-out of its production by the Montreal Protocol. Nevertheless, this atmospheric concentration decline suffered a slow-down around 2012 due to emissions from non-reported production. Since CFC-11 is one of the most important ozone-depleting chlorofluorocarbons (CFCs), its continuous monitoring is essential. We present the CFC-11 total column time series (2000–2020) retrieved in a consistent way from ground-based high-resolution solar absorption Fourier transform infrared (FTIR) spectra. These observations were recorded at two remote stations of the Network for the Detection of Atmospheric Composition Change (NDACC): the Jungfraujoch station (Northern Hemisphere) and the Lauder station (Southern Hemisphere). These time series are new. They were produced using improved line parameters and merged considering the instrument changes and setup modifications. Afterwards, they were compared with Cape Grim station *in situ* surface observations conducted within the Advanced Global Atmospheric Gases Experiment (AGAGE) network and with total column datasets calculated by the TOMCAT/SLIMCAT 3-D chemical transport model. Trend analyses were performed, using an advanced statistical tool, in order to identify the timing and magnitude of the trend change in both hemispheres. The observations are consistent with the model results and confirm the slowdown in the CFC-11 atmospheric concentration decay, since ≈2011 in the Northern Hemisphere, and since ≈2014 in the Southern Hemisphere.

Environmental significance

CFC-11 is one of the most important chlorofluorocarbons (CFCs) emitted into the atmosphere. CFCs are chemicals, exclusively produced by human activities. When CFC-11 is transported into the stratosphere, it is photodissociated, releasing chlorine atoms that catalytically destroy stratospheric ozone, which protects the biosphere from harmful UV radiation. The main aim of this manuscript is to show that ground-based FTIR instruments are relevant to measure changes in atmospheric CFC-11 concentrations. This manuscript is in support of the Montreal Protocol on Substances that Deplete the Ozone Layer. We demonstrate that the FTIR instruments are a good complement to *in situ* and satellite measurements, since we could confirm the slowdown in the CFC-11 atmospheric concentration decay, related to the non-declared emissions.

[a]*Department of Astrophysics, Geophysics and Oceanography, UR SPHERES, Université de Liège, Liège, 4000, Belgium. E-mail: i.pardocantos@uliege.be*
[b]*School of Earth and Environment, University of Leeds, Leeds, UK*
[c]*National Centre for Earth Observation, University of Leeds, Leeds, UK*
[d]*National Institute of Water and Atmospheric Research Ltd., Lauder, New Zealand*
[e]*Atmospheric Chemistry Observations and Modeling, National Center for Atmospheric Research, Boulder, CO 80305-5602, USA*
[f]*Department of Econometrics and Data Science, Vrije Universiteit Amsterdam, Amsterdam, Netherlands*
[g]*Climate Science Centre, CSIRO Oceans and Atmosphere, Aspendale, Victoria, Australia*
[h]*Department of Earth, Space and Environment, Chalmers University of Technology, Gothenburg, Sweden*
[i]*Institute of Environmental Physics, University of Bremen, Bremen, 28359, Germany*
[j]*Department of Astrophysics, Geophysics and Oceanography, UR STAR, Université de Liège, Liège, 4000, Belgium*

1. Introduction

Trichlorofluoromethane (CFC-11) is one of the most important chlorofluorocarbons (CFCs) emitted into the atmosphere. CFCs are chemicals exclusively produced by human activities and they were used as aerosol spray propellants, refrigerants, inflating and insulating agents in the production of foam materials, and solvents.[1] CFC-11 is transported into the stratosphere where it is photodissociated by UV radiation, releasing chlorine atoms that catalytically destroy stratospheric ozone.[2] Therefore, CFC-11 has substantially contributed to the buildup of organic and inorganic chlorine, and subsequently the stratospheric ozone depletion, which was first reported by Farman *et al.*, 1985.[3] Its mean atmospheric lifetime is 52 years (uncertainty range of 43–67 years),[4] and residual banks will continue emitting CFC-11 for some decades before complete removal from the atmosphere can be expected.[5] Thus, this molecule is an important target to monitor at present even though its emissions have decreased noticeably in response to production phase-down measures introduced by the Montreal Protocol on Substances that Deplete the Ozone Layer (1987) and its subsequent amendments and adjustments.[6]

Due to the Montreal Protocol, the tropospheric concentrations of CFC-11 reached a maximum around 1994 and decreased afterwards.[6] Although it was decided to almost completely phase out CFC production by 2010, Montzka *et al.*, 2018 [7] reported that the decrease in atmospheric CFC-11 concentrations suffered a slowdown since 2012 in both hemispheres, due to an unexpected increase of its emissions, evaluated at (13 ± 5) Gg per year since 2012. Emissions from this illegal CFC-11 production are mainly coming from eastern China, as reported by Rigby *et al.*, 2019.[8] The Atmospheric Chemistry Experiment (ACE) satellite measurements have shown that the tropospheric rate of decrease, between 60°S and 60°N, has changed from (−1.81 ± 0.05) ppt per year (2004–2012) to (−1.16 ± 0.04) ppt per year (2012–2020)[9] (see green line in Fig. 1). Consequently, this slowdown in the decrease of CFC-11 atmospheric concentrations is expected to produce a delay in ozone recovery.[10] Fortunately, Montzka *et al.*, 2021 [11] and Park *et al.*, 2021 [12] have reported a return to reduced emission rates levels, similar to that during 2008–2012 since 2018.

In this work, we analyse the CFC-11 abundances above the Jungfraujoch and Lauder stations along with ground level *in situ* concentrations from Cape Grim. Here, the Lauder total column CFC-11 decadal datasets were analysed for the first time and, in order to better characterise the CFC-11 decadal trend at Jungfraujoch, the time series was harmonised and updated, improving the datasets presented in previous assessments.[4,6] We focus on the period from January 2000 to December 2020 to analyse the influence in Europe, and Southern Hemisphere mid-latitudes, of the emissions related to the new, illegal production. In order to do so, we compare the FTIR total columns with TOMCAT/SLIMCAT chemical transport model data for three different simulations of differing CFC-11 emission rates. In Section 2, we describe the FTIR and the *in situ* observations, and the 3-D chemical transport model. In Sections 3 and 4, we present the FTIR CFC-11 retrieval strategy, then we show the results of the trend analyses, for the Jungfraujoch (Northern Hemisphere, NH) and the Lauder and Cape Grim (Southern Hemisphere, SH) stations, as well as the respective model trend analyses. Finally, we present the conclusions of our study in Section 5.

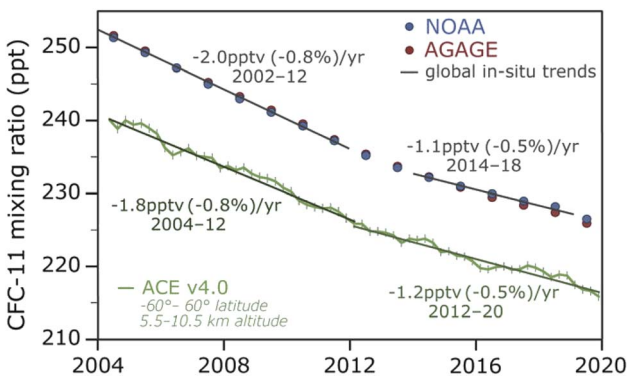

Fig. 1 CFC-11 global mixing ratio and trends from the ACE-FTS instrument (60°N to 60°S) in green (4 months means) and from *in situ* measurements (annual means): NOAA in blue, and AGAGE in red. Fig. 2.2(b) of the Report on the Unexpected Emissions of CFC-11, 2021.[4]

2. CFC-11 ground-based high-resolution IR observations, *in situ* observations, and 3-D model

In this study, we used data from three mid-latitude stations, Jungfraujoch at 46.55°N, Lauder at 45.04°S, and Cape Grim at 40.68°S. The Jungfraujoch and Lauder FTIR measurements are taken under the auspices of the Network for the Detection of Atmospheric Composition Change (NDACC),[13] and the Cape Grim *in situ* sampling are conducted within the framework of the Advanced Global Atmospheric Gases Experiment (AGAGE) global network.[14]

2.1 The Jungfraujoch station FTIR observations

The High Altitude Research Station Jungfraujoch (46.55°N, 7.98°E) is located on the Northern Swiss Alps, on a saddle between the Mönch and the Jungfrau summits, at 3580 m above mean sea level (a.m.s.l.), thus the station is most of the time in free troposphere conditions.[15]

The Institute of Astrophysics of the University of Liège has collected infrared (IR) solar spectra at that site since the early 1950s. Firstly, grating spectrometers were used and then two Fourier-Transform Infrared (FTIR) spectrometers have run since the mid-1980s, a homemade instrument (from 1984 to 2008), and a commercial Bruker IFS-120HR spectrometer (from the beginning of the 1990s to present). The optical filters and the HgCdTe (mercury cadmium telluride, MCT) or InSb (indium antimonide) cooled detectors allow to cover the mid-IR spectral range. See Zander *et al.*, 2008 [16] for more information about the instrumentation. The IR solar absorption spectra used in this study were recorded by the homemade and the Bruker

instruments, with a HgCdTe detector, under clear-sky conditions. These spectra cover the 700–1400 cm^{-1} range with a spectral resolution of 0.0061 cm^{-1}, what corresponds to a maximum optical path difference (OPD) of 82 cm. The mean signal-to-noise ratio (SNR) of the studied period (2000–2020) is 945.

2.2 The Lauder station FTIR observations

Like Jungfraujoch, the Lauder Atmospheric Research Station (45.04°S, 169.68°E, 370 m a.m.s.l.) was a founding site of NDACC. Mid-IR FTIR measurements started at Lauder in the early 1990s and continue to the present day. The spectral observations used in this study were recorded with a Bruker 120HR (2000–2018) and Bruker 125HR (2018–2020). In both instruments, solar spectra (covering the region 700–4000 cm^{-1}) are taken on days with cloud-free line of sight to the Sun using solar trackers with active tracking.[17] Solar spectra used in the retrieval of CFC-11 were taken with a HgCdTe detector through a mid-IR bandwidth filter 700–1400 cm^{-1}, at a spectral resolution of 0.0035 cm^{-1} using a KBr beamsplitter. Such spectra are also used in the analysis of other trace gases species, such as O_3,[18] HNO_3,[19] and $ClONO_2$.[20] Instrument line shape and alignment are monitored monthly using low pressure HBr and N_2O cells.[21,22]

2.3 The Cape Grim station *in situ* observations

In situ observations of CFC-11 commenced at Cape Grim, Tasmania (40.7°S, 144.7°E), in 1976 and have continued uninterrupted until the present day.[23,24] The station, operated by the Australian Bureau of Meteorology, sits atop a 90 m cliff on Tasmania's west coast and the ambient air is sampled 36 times per day from a tower at 70 m above the station. The Cape Grim CFC-11 baseline monthly mean data (2001–2020) reported in this paper are obtained from CSIRO's participation in the global AGAGE program.[14] The data were obtained from a gas chromatographic (GC) instrument incorporating an electron capture detector (ECD) and are calibrated in the Scripps Institution for Oceanography (SIO-05) scale. Baseline data are selected using a statistically-based algorithm, and are free of the influence of regional CFC-11 emissions and represent mid-latitude, background CFC-11 mixing ratios for the Southern Hemisphere.[14]

2.4 TOMCAT/SLIMCAT chemical transport model

TOMCAT/SLIMCAT (hereafter TOMCAT) is a global 3-D off-line chemical transport model.[25] It is used to study a range of chemistry-aerosol-transport issues in the troposphere and stratosphere. The model is usually forced by European Centre for Medium-Range Weather Forecasts (ECMWF) meteorological (re)analyses, although General Circulation Model (GCM) output can also be used. When using ECMWF fields, as in the experiments described here, the model reads in the 6-hourly fields of temperature, humidity, vorticity, divergence and surface pressure. The resolved vertical motion is calculated online from the vorticity. For the simulations used in this study, the model was run at horizontal resolution of 2.8° × 2.8° with 60 hybrid σ-pressure levels from the surface to ≈60 km. The model was run from 1980 to 2020 and forced by ECMWF ERA5 reanalyses.[26] Convective mass fluxes were calculated online using the scheme of Tiedtke, 1989 [27] and mixing in the boundary layer is based on the scheme of Holtslag and Boville, 1993.[28] The model simulations included three idealised CFC-11 tracers, as used in Montzka *et al.*, 2021.[11] The simulation parameterised the atmospheric loss of the CFC-11 tracers using calculated photolysis rates and a repeating year of archived monthly mean zonal mean O (^1D) distributions from a previous full chemistry simulation. Tracer A used the best estimate of historic CFC-11 emissions with realistic distribution at the surface.[11] Tracer B used the same total time-dependent emissions as tracer A but they were distributed uniformly over the Earth's surface. Tracer C assumed zero CFC-11 emissions after 2000.

3. CFC-11 vertical column retrieval

3.1 Retrieval strategy

At both, Jungfraujoch (JFJ) and Lauder (LAU), column retrievals were performed with the SFIT-4 v0.9.4.4. algorithm which implements the Optimal Estimation Method (OEM) of Rodgers, 2000.[29] For the Jungfraujoch station, the layer scheme contained 41 layers from 3.58 km to 120 km, whereas the Lauder station layering scheme spanned 47 layers from 0.37 km to 120 km. In both schemes, the thicknesses gradually increased from 0.65 km (JFJ) and 0.43 km (LAU) for the lowermost layer up to 14 km for the top one.

Since the CFC-11 has a very broad but relatively unstructured absorption in the infrared spectral range, the retrieval spectral window has to be relatively large to encompass the whole feature. Furthermore, it has to be carefully optimised in order to limit the interference by other molecules. The optimal spectral window for CFC-11 was first defined by Zander *et al.*, 1983 [30] as 825–860 cm^{-1}. For this study, it was adjusted to 830.0–859.3 cm^{-1} in order to avoid a H_2O absorption line at ≈859.5 cm^{-1}; and only the observations with an apparent solar zenith angle (SZA) between 60° and 85° (JFJ), and between 60° and 89° (LAU) were fitted such as to maximize the CFC-11 absorption depth and information content.

The interfering telluric species used in this retrieval strategy were H_2O, CO_2, O_3, OCS, HNO_3, $COCl_2$, and $H_2{}^{18}O$, and their spectroscopic parameters were taken from the HITRAN2008 [31] and HITRAN2012 [32] molecular spectroscopic databases, the ATM2019 molecular spectroscopic database (**https://mark4sun.jpl.nasa.gov/specdata.html**) or the empirical pseudo-linelist (PLL) created by G. C. Toon (**https://mark4sun.jpl.nasa.gov/pseudo.html**). PLLs are appropriate to model unresolved features, as those of CFC-11 and $COCl_2$. Solar lines were obtained from the empirical model proposed by Hase *et al.*, 2006.[33] At Lauder, spectral channeling of ≈0.1% amplitude (caused by filter etalon) was also fitted.

We adopted an OEM regularization since it allowed to retrieve more information compared to a Tikhonov-type regularization. The diagonal elements of the *a priori* covariance matrix, S_a, were set to 15% per km. For the off-diagonal terms, we took an interlayer correlation half-height half-width (of exponential-shape correlation) of 4 km. The signal-to-noise

ratio for the inversions was established to 100 for JFJ and 180 for LAU.

At JFJ and LAU, *a priori* CFC-11 and all interfering species profiles were calculated from a climatology of the Whole Atmosphere Community Climate Model (WACCM, version 4 (ref. 34)) simulations for the 1980–2020 period, except for water vapour at JFJ. *A priori* water vapour profiles for JFJ were provided by the ERA-Interim[35] meteorological reanalyses extrapolated for the top of the atmosphere using WACCM monthly means (2000–2019). Since the ERA-Interim reanalysis is only available until August 2019, we used the reanalyses from the National Centers for Environmental Prediction (NCEP)[36] for the final period. Atmospheric pressure and temperature profiles were also supplied by NCEP.

Fig. 2 shows the synthetic spectra produced by the SFIT-4 algorithm for CFC-11 and the main interfering species at the selected spectral window for the Jungfraujoch station. The top panel displays residuals (%) from the fit to a spectrum recorded on 8th January 2008. The bottom panel shows the simulated spectrum (black line) and the per-species spectra for our target and the main absorbers in this range (H_2O, CO_2, and O_3) as well as the solar spectrum. Note that the interfering species and solar spectra are offset vertically for clarity. A good fit is obtained in this wide spectral range, with residuals close to the noise level, except near some of the strongest water vapour lines. It is worth noting that this good agreement is representative of the whole Jungfraujoch fitting residuals since the root-mean-square of the fitting residuals (RMS) for this example is 0.20%, the median RMS for the entire time series is 0.23%, and the mean RMS is (0.25 ± 0.07)%.

3.2 Error budget and information content of measurements

Table 1 shows the main sources of error (measurement, temperature, interfering species, *etc.*) affecting the retrieval of Jungfraujoch and Lauder CFC-11 total columns, calculated for one year (2008 and 2016, respectively) of observations. Every error includes both a systematic and a random component. As described in eqn (8) of Zhou *et al.*, 2016 [37] the total error contains four different parts: the smoothing error, the forward model error, the measurement error, and the forward model parameter error.[37]

To calculate the smoothing error (eqn (3.16) of Rodgers, 2000 [29]), we produced the random component of the error covariance S_b matrix by calculating the relative standard deviation in version 4.0 Level 2 CFC-11 ACE-FTS[38] retrievals, for each level of the grid (14.5–22.5 km between 40 and 50°N), for the 02/2004 to 02/2020 period. The S_b matrix systematic part was created using the mean relative difference of CFC-11 retrievals between ACE-FTS and MIPAS Level 2 Version 8.22 (ref. 39) for each layer (from 05/2005 to 04/2012). The CFC-11 profile correlation width was set to 4 km. For the solar zenith angle at the JFJ station, the random uncertainty was assumed as ±0.15° and the systematic uncertainty as ±0.1°. For the Lauder station, all SZA uncertainty was assumed random. According to the empirical PLL, the relative systematic uncertainties of CFC-11 spectroscopic parameters were set to 7%.

The total random errors are 3.3% and 2.17%, for the Jungfraujoch and Lauder stations respectively, and they are mostly influenced by the temperature profile uncertainties. The total

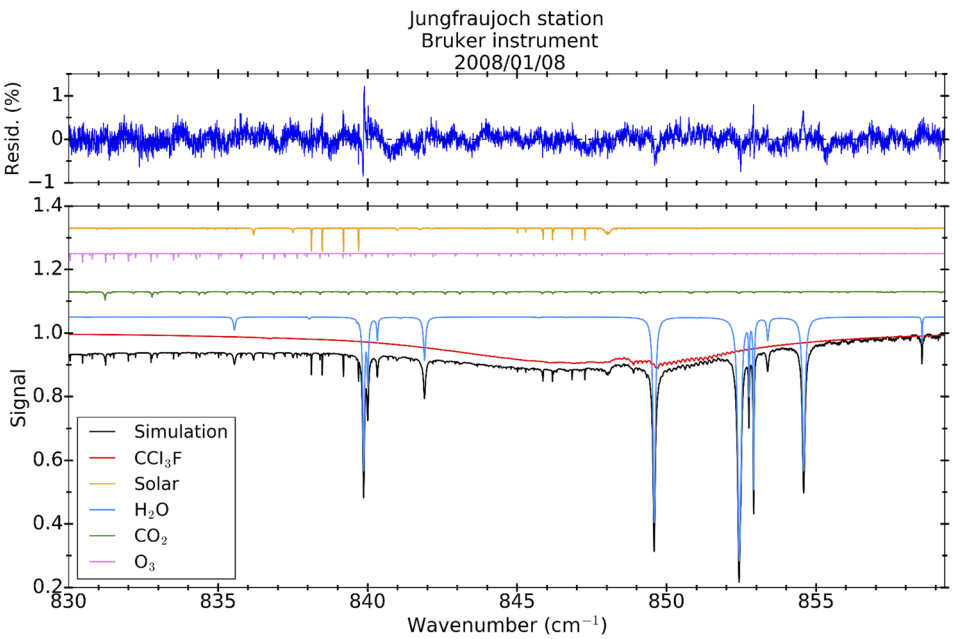

Fig. 2 Simulations of the 830.0–859.3 cm^{-1} spectral window from spectra recorded by the Bruker IFS-120HR FTIR instrument at Jungfraujoch station with an apparent solar zenith angle of 80.3°, and a maximum optical path difference of 82 cm. The root-mean-square of the fitting residuals (RMS) is 0.20%. The main interfering species (H_2O, CO_2, and O_3) and the solar spectra are shifted vertically for clarity. Second-order absorbers are not shown. The top panel displays the observed-calculated residuals, in %, from the fit to the spectrum recorded on 8 January 2008.

Table 1 Mean relative errors (%) that concern the total column retrievals of CFC-11 for the Jungfraujoch (JFJ) and Lauder (LAU) stations

	Relative uncertainty (%)		
Error type and source	JFJ	LAU	Notes
Random components			
Measurement	0.9	0.7	Assuming ± 0.15° for solar pointing (JFJ) and 0.025° half diameter at max (LAU)
Temperature	2.7	2.0	
SZA	1.16	0.15	
Zero-level offset (zshift)	1.1	0.01	
Interfering species	0.13	0.05	
Smoothing	0.4	0.4	
Retrieval parameters	0.02	0.01	
Total random	**3.3**	**2.2**	
Systematic components			
CFC-11 line intensity	7	7.1	Assuming 7% from pseudo-linelist
Temperature	2.11	0.34	
SZA	0.8	0.0	Assuming ± 0.10° for solar pointing (JFJ); all SZA is assumed random (LAU)
Zero-level offset (zshift)	1.1	0.0	All zshift is assumed random (LAU)
Retrieved interfering species (*i.e.* H_2O) line intensity	0.02	0.01	
Total systematic	**7.5**	**7.2**	

systematic errors are 7.5% and 7.2%, for the Junfraujoch and Lauder stations respectively, and they are dominated by the uncertainty in the spectroscopic parameters on the intensities of the pseudo-lines fitted to the cross-section laboratory spectra, and in the temperature profile uncertainty. Uncertainties agree with those obtained by Zhou *et al.*, 2016 [37] (Reunion Island) and Polyakov *et al.*, 2021 [40] (St. Petersburg). The other sources of uncertainty (random and systematic) only contribute to the total error at 1% (*i.e.* zshift) or less (*i.e.* interfering species).

In order to evaluate the information content of the retrieval processing, the mean averaging kernels were analysed. The averaging kernel matrix (A) described in the Rodgers formalism[29] characterises the contribution of the *a priori* (x_a) and the true (x) vertical distributions to the retrieved vertical profile ($\hat{x}$). According to eqn (3.12) of Rodgers, 2000:[29]

$$\hat{x} = x_a + A(x - x_a) + G_y e_y \quad (1)$$

where $G_y e_y$ is the error in the retrieval originated by the total measurement error (retrieval error).

Fig. 3 shows the mean layer averaging kernels (left) and eigenvectors (right) derived from the retrievals of the 2004–2006 spectra in the case of Jungfraujoch (panels (a) and (b)) and the 2017–2020 spectra for Lauder (panels (c) and (d)). The coloured lines in the averaging kernel plots show the different individual layer averaging kernels, and the black line shows the total column averaging kernel (scaled by 0.1), from the site altitude (3.58 km for Jungfraujoch and 0.37 km for Lauder) up to 40 km.

The degrees of freedom for signal (DOFS) is a measure of independent information in the retrieved profile and is defined as the trace of the averaging kernel matrix (Tr(A)) or the sum of eigenvalues.[29] For Jungfraujoch, mean DOFS is 1.36, meaning that one piece of information can be obtained from the retrievals. The first eigenvalue indicates that 99% of the information characterising the troposphere comes from the retrieval, and not from the adopted *a priori* profile. As to the second eigenvalue, it amounts on average to 0.35, preventing the determination of two independent pieces of information, or partial columns, above and below about 8 km. However, the second eigenvector still allows to improve height resolution. Concerning Lauder results, the DOFS is 1.57 and the first eigenvalue is 1.00, indicating that 100% of the information describing the troposphere is coming from the retrievals. The second eigenvalue, equal to 0.56, shows that two columns (tropospheric and lower-stratospheric) can be separated at 5.3 km with almost 60% of the information coming from the retrievals.

4. Results

In this section, we present the harmonised Jungfraujoch FTIR dataset, the merged Lauder FTIR dataset and the Cape Grim *in situ* measurements. We performed trend analyses on these datasets from both hemispheres as well as on model data, with the purpose of comparing them and drawing some conclusions.

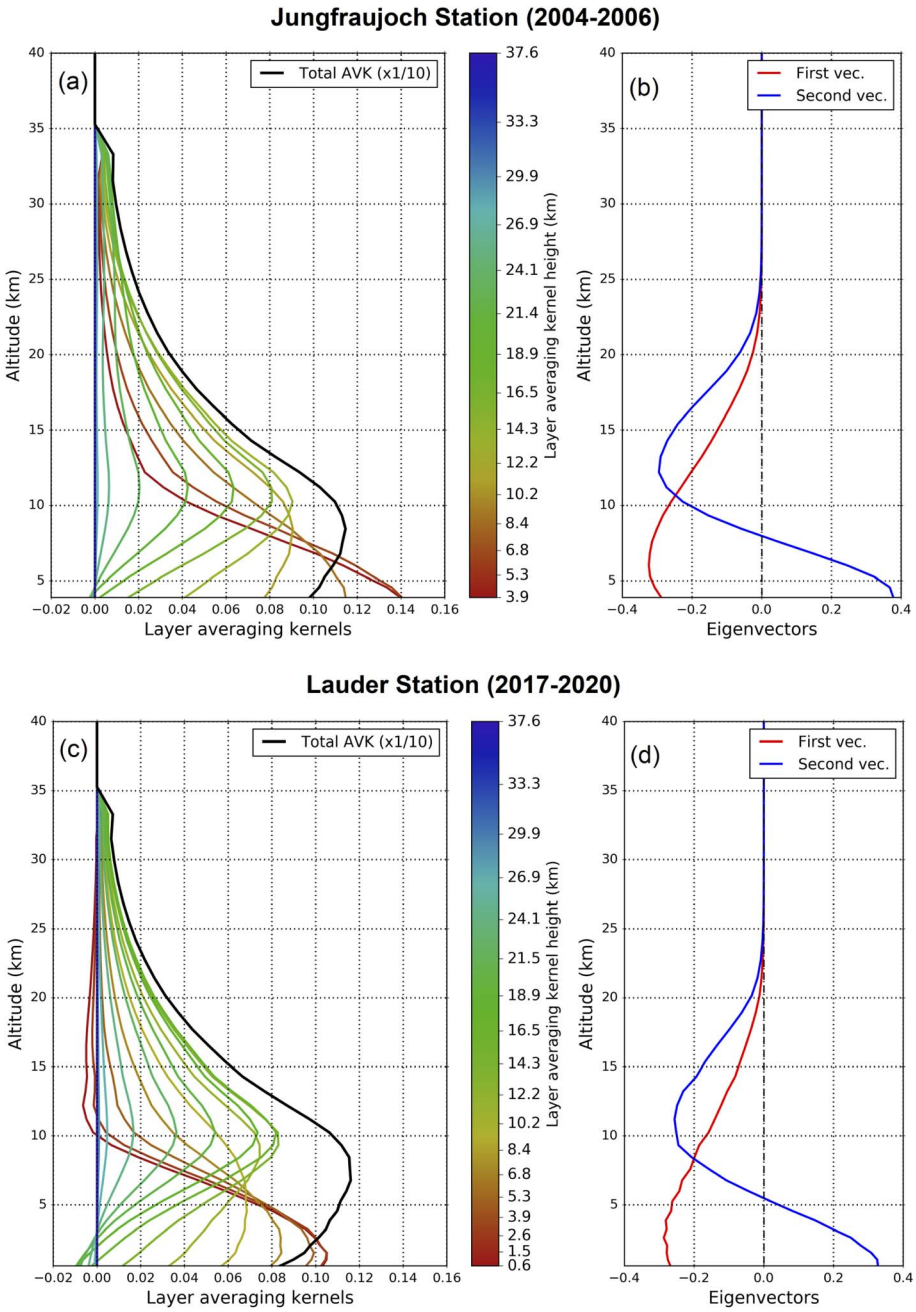

Fig. 3 (a) Mean layer averaging kernels for mixing ratios computed for the spectra recorded (a) from January 2004 to December 2006 above Jungfraujoch and (c) from November 2017 to December 2020 above Lauder. The ticks on the colour bar are the individual layer averaging kernels represented in the plots. Eigenvectors are shown in (b) for Jungfraujoch and in (d) for Lauder. The two first eigenvalues are (b) 0.99 and 0.35, respectively, and (d) 1.00 and 0.56, respectively.

4.1 FTIR Jungfraujoch time series analysis

The 6921 Jungfraujoch spectra used for our study were recorded over 2055 sunny days between 25th June 1986 and 10th December 2020. Specifically, we have analysed the trend between January 2000 and December 2020 using monthly means (1699 days and 244 months).

In order to obtain the whole time series shown in Fig. 4, we had to harmonise the daily total columns since two different instruments were used. Furthermore, several changes were progressively implemented to the Bruker spectrometer, potentially affecting the instrumental response and thus also the CFC-11 retrieved columns. This is particularly true when a broad window is used, as is also the case for peroxyacetyl nitrate (PAN).[41] The first adjustment was to harmonise the two instruments (homemade and Bruker) time series by multiplying the Bruker time series by a factor of 0.9692 between 12/02/1999 and 09/10/2001. Afterwards, we multiplied the homemade instrument whole time series by a factor of 0.9467. These

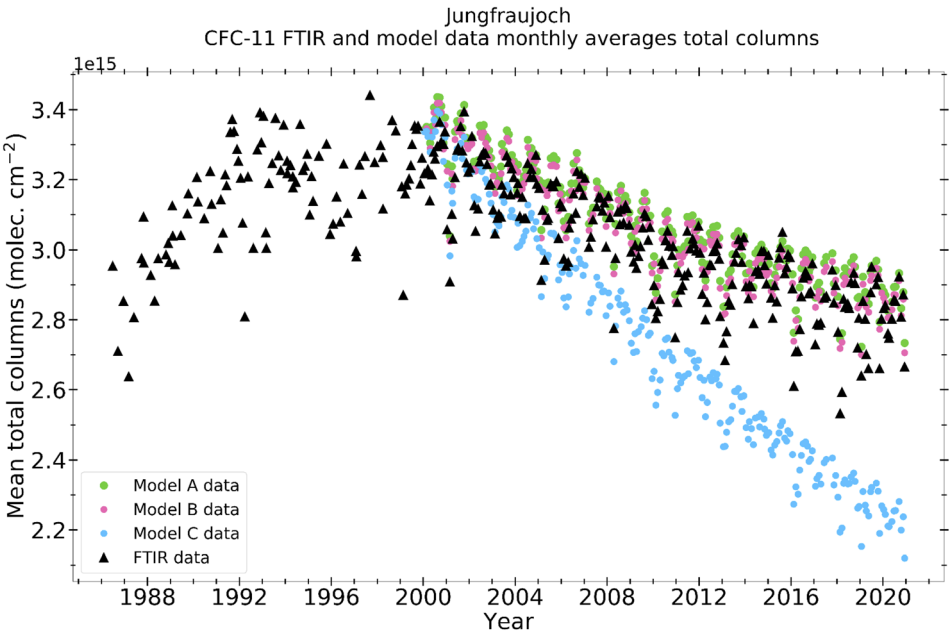

Fig. 4 Jungfraujoch FTIR (from June 1986 to December 2020) and TOMCAT monthly mean total columns (from January 2000 to December 2020). In black, FTIR data; in green, TOMCAT model simulation A: best estimate of emissions and some realistic distribution (optimized with NOAA support); in pink, TOMCAT model simulation B: same total emissions as simulation A but equal emissions at all lat/lon; and in blue, TOMCAT model simulation C: zero emissions since 2000 (simple decay).

correction factors were found by comparing the coincident data present in the two subsets (homemade and Bruker) for the same days. Nevertheless, there was still a non-scaled period from 16/10/2015 to 18/06/2019, found to be inconsistent because of the change of one spectrometer mirror in the Bruker instrument. Thus, they were scaled up (factor of 1.0181) so as to get the optimum alignment of this subset with respect to the earlier and following column data. These corrections allowed us to acquire the harmonised series from June 1986 to December 2020 shown in Fig. 4.

4.2 FTIR Lauder time series analysis

At Lauder, 4907 FTIR spectra were recorded over 1685 sunny days (225 months), from 11th October 2001 to 27th December 2020. As we did with the JFJ time series, we have analysed the trend between October 2001 and December 2020 using monthly means.

The Lauder Bruker 120HR spectrometer was replaced in 2018 by a Bruker 125HR and, as observed in the Jungfraujoch time series, this kind of change can affect the instrumental response and the retrieved quantities. Therefore, we used the common days of observation between both instruments to estimate a correction factor in order to merge both datasets (Bruker 120HR and Bruker 125HR). We found a 1.4% difference, thus we multiplied the 125HR time series by this factor. The final xCFC-11 time series is shown in Fig. 6(a).

Within the Lauder time series, there were unexpectedly high CFC-11 total columns between 2007 and 2009.5. For the purpose of finding the main cause of this time series feature, several hypotheses were tested. Firstly, we analysed the xCFC-11 time series since the Lauder station is a relatively low-altitude site and it is strongly influenced by water vapour. The unexpectedly high points were also present in the xCFC-11 amounts. Secondly, we analysed the *in situ* mixing ratio CFC-11 time series (blue points in Fig. 6(a)) at Cape Grim (Tasmania, Australia) from October 2001 to September 2020. The Cape Grim time series did not show a shape of that sort. Therefore, we continued investigating by analysing the FTIR CFC-12 (CCl_2F_2) and N_2O total columns above Lauder, since they are a co-emitted species and a dynamical tracer, respectively. These species did not show any anomalies.

A series of tests were performed to assess the robustness of the retrieval strategy. This involved investigating the effect of MCT detector non-linearity (saturation point fitting), instrument response function changes and fitting of the broad retrieval window continuum level. In all tests, the unexpectedly high abundances over 2007–2009.5 were still present, and the linear trend analysis results were not significantly altered (details in Section 4.3.2). Even though we presently cannot find fault with the measurements and retrieval strategy, the anomalous values cannot be reconciled with CFC-11 emission rates or transport/dynamic circulation changes, thus the cause for this feature still remains unresolved.

4.3 Trend analyses

The time series trends presented in this section were obtained using the auto-regressive wild bootstrap (AWB) method developed by Friedrich *et al.*, 2020.[42,43] This method first tests for the presence of a break point in the trend function. If there is evidence of a break, it locates the break point that best fits the

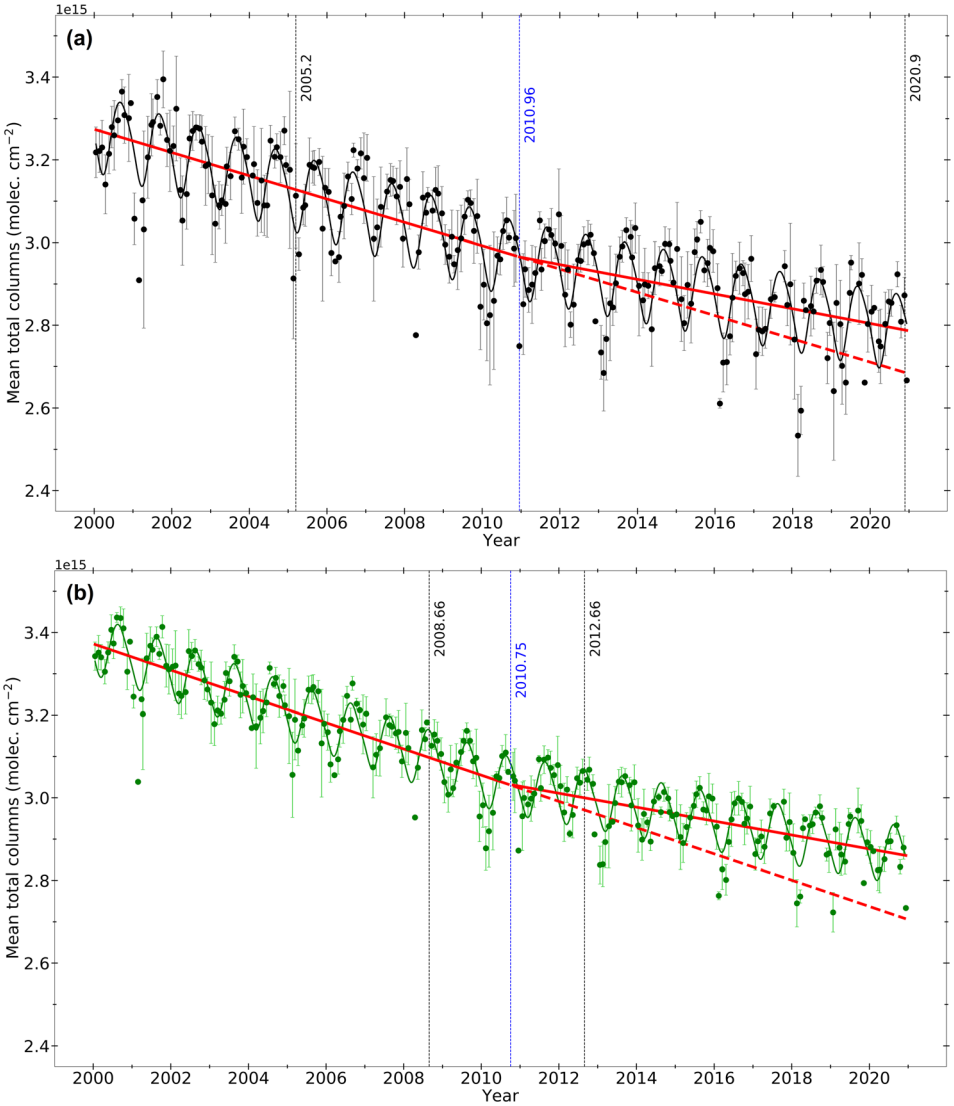

Fig. 5 (a) FTIR and (b) TOMCAT monthly time series of CFC-11 total columns above Jungfraujoch. All vertical bars represent the standard deviations around the monthly means. (a) Total columns have been derived from solar spectra recorded by the Bruker IFS 120HR spectrometer. (b) The "best estimation/realistic" simulation (tracer A) has been chosen.

data (where the fit is determined by the sum of squared deviations from the broken trend line). Then, it determines the uncertainty around the break location using the AWB method. It also estimates the pre- and post-break trends slopes using ordinary least squares (OLS) and judges the significance of the estimated trend slopes using the bootstrap method. We used a 95% confidence interval.

4.3.1 Northern Hemisphere. The FTIR Jungfraujoch monthly mean total columns from January 2000 until December 2020 are displayed in Fig. 5(a) with the error bars showing the standard deviation around the monthly means. The mean relative standard deviation is 2%, *i.e.*, lower than the random uncertainty reported in Table 1. We performed a linear trend analysis of all the data (2000–2020). We found that the CFC-11 atmospheric concentration decreased by $(2.34 \pm 0.14) \times 10^{13}$ molecules per cm^2 per year, or a relative decrease of (0.78 ± 0.05)% per year. Since Montzka *et al.*, 2018 [7] reported a slowdown in the decrease of the atmospheric CFC-11 concentrations, we used the Friedrich *et al.*, 2020 [42,43] approach in order to find the break location and estimate the trend change. We found a statistically significant break point around 2011. The blue vertical line in Fig. 5(a) indicates the break point at 2010.96, and a large confidence interval varying within 2005.20 and 2020.90 is indicated by the two black vertical lines. The pre-break slope (*i.e.*, from 2000 until ≈2011) is $(-2.87 \pm 0.39) \times 10^{13}$ molecules per cm^2 per year, representing a relative decrease of (0.95 ± 0.13)% per year; while the post-break (2011–2020) trend decrease is $(1.84 \pm 0.44) \times 10^{13}$ molecules per cm^2 per year, that is a relative trend of (-0.61 ± 0.15)% per year. This trend change of around 56% is significant at the 2σ level of uncertainty. This trend change is in good agreement with the trend change estimated from the ACE-FTS mixing ratios trend values reported by Bernath *et al.*, 2020,[9] as well as from the NOAA and AGAGE data, as shown in Fig. 1. The red

dashed line shows the divergence between an unperturbed situation and the current rate of change of CFC-11 following the recent renewed emissions.

The FTIR time series is compared to TOMCAT model outputs for the Jungfraujoch station location. Three different scenarios were carried out for the January 2000 to December 2020 period. We chose the scenario with the best estimate of emissions and the most realistic distribution (run A). In Fig. 5(b), we can see that the break location is found at 2010.75, with a confidence interval ranging from 2008.66 to 2012.66, which lies within the confidence interval obtained for the break point in the FTIR time series. The standard deviation around the monthly means is shown by the error bars and the mean relative standard deviation is 1.5%, which is lower than for the FTIR measurements. Model data are not affected by random noise as are the measurements. The pre-break trend is $(-3.18 \pm 0.25) \times 10^{13}$ molecules per cm^2 per year, *i.e.*, (-1.03 ± 0.08)% per year, whereas the slope is $(-1.69 \pm 0.29) \times 10^{13}$ molecules per cm^2 per year ((-0.55 ± 0.09)% per year) for the post-break period.

Since the Lauder and Cape Grim stations are relatively low-altitude sites, they are influenced by water vapour. In order to create comparable datasets in both hemispheres, we analysed the FTIR dry air mole fraction (xCFC-11) trends (for JFJ and LAU). The xCFC-11 is computed by dividing the CFC-11 total columns by the dry air pressure column (DPC).[44] The DPC is calculated by using the ground pressure of the station location (here the Jungfraujoch station, and in Section 4.2.2 the Lauder station) to calculate column air concentrations, according to the eqn (1) of Barthlott *et al.*, 2015:[44]

$$\mathrm{DPC} = \frac{P_s}{M_{\mathrm{dryair}} \cdot g(\phi)} - \frac{M_{H_2O}}{M_{\mathrm{dryair}}} \cdot H_2O_{\mathrm{col}} \quad (2)$$

where P_s is the surface pressure (in Pa), $g(\phi)$ is the latitude-dependent surface acceleration due to gravity (at the station location), M_{dryair} is the molecular mass of the dry air ($\approx 28.96 \times 10^{-3} N_A$ kg per molecules), M_{H_2O} is the molecular mass of the water vapour ($\approx 18 \times 10^{-3} N_A$ kg per molecules), N_A is the Avogadro's constant ($\approx 6.022 \times 10^{23}$ molecules per mol), and H_2O_{col} is the water vapour total column amount (in molecules per m^2).

The xCFC-11 FTIR trend for the whole Jungfraujoch time series is $(-1.70 \pm 0.08) \times 10^{13}$ ppt per year, *i.e.*, (-0.79 ± 0.04)% per year. The break point for the xCFC-11 time series was found at 2010.92 with a confidence interval extending from 2007.00 to 2016.25. Before the break, the trend decreases by (2.01 ± 0.18) ppt per year, which is a relative trend of (-0.79 ± 0.04)% per year; while the post-break trend is $(-1.35 \pm 0.23) \times 10^{13}$ ppt per year, *i.e.*, (-0.66 ± 0.11)% per year. This leads to a trend change of around 36%. All the trend estimates in Table 2 show the excellent agreement between the FTIR and the model data above the Jungfraujoch station.

We have also analysed the 06/1986 to 12/1992 trend preceding the plateau (see Fig. 4) in the FTIR Jungfraujoch data. This upward trend is $(7.27 \pm 1.67) \times 10^{13}$ molecules per cm^2 per year, *i.e.*, (2.35 ± 0.54)% per year. In this case, due to the small number of monthly data of this period, we carried out the trend analysis using the daily data. These results are in agreement with the trends calculated from the atmospheric histories for CFC-11 for this period (2.53% per year).[45] These historical values were determined from experimental observations made by the Atmospheric Lifetime Experiment/Global Atmospheric Gases Experiment/Advanced Global Atmospheric Gases Experiment (ALE/GAGE/AGAGE) network at the Northern Hemisphere.

4.3.2 Southern Hemisphere. The monthly xCFC-11 above Lauder, as well as the *in situ* monthly CFC-11 at Cape Grim and model data, are shown in Fig. 6. Error bars indicate the standard deviation around the monthly means. The average relative standard deviation is 1.6% for the Lauder data, 0.08% for the Cape Grim data, and 1.4% for the model data.

The break location is found at 2014.13 for Lauder and at 2014.69 for Cape Grim time series. The ranges for the confidence interval are shown by the dashed vertical lines: the black ones correspond to the Lauder data, while the blue ones show the Cape Grim confidence interval. Comparing these results to the model time series (Fig. 6(b)), we can see that the break point

Table 2 xCFC-11 (not shown in the plots) and CFC-11 total columns annual trends derived from the Jungfraujoch FTIR time series and TOMCAT model

	2000–2020	Break location	2000 to Break	Break to 2020	
xCFC-11 FTIR JFJ	-1.70 ± 0.08	2010.92	-2.01 ± 0.18	-1.35 ± 0.23	Dry air mole fraction trends (ppt per year)
	-0.79 ± 0.04		-0.90 ± 0.08	-0.66 ± 0.11	Relative trends (% per year)
CFC-11 FTIR JFJ	-2.34 ± 0.14	2010.96	-2.87 ± 0.39	-1.84 ± 0.44	Total columns trends (10^{13} molecules per cm^2 per year)
	-0.78 ± 0.05		-0.95 ± 0.13	-0.61 ± 0.15	Relative trends (% per year)
xCFC-11 TOMCAT for JFJ (tracer A run)	-1.80 ± 0.05	2010.38	-2.29 ± 0.10	-1.34 ± 0.09	Dry air mole fraction trends (ppt per year)
	-0.82 ± 0.02		-1.04 ± 0.04	-0.61 ± 0.04	Relative trends (% per year)
TOMCAT for JFJ (tracer A run)	-2.47 ± 0.11	2010.75	-3.18 ± 0.25	-1.69 ± 0.29	Total columns trends (10^{13} molecules per cm^2 per year)
	-0.80 ± 0.04		-1.03 ± 0.08	-0.55 ± 0.09	Relative trends (% per year)
xCFC-11 TOMCAT for JFJ (tracer C run)	-3.90 ± 0.06	—	—	—	Dry air mole fraction trends (ppt per year)
	-2.00 ± 0.03				Relative trends (% per year)
TOMCAT for JFJ (tracer C run)	-5.44 ± 0.11	—	—	—	Total columns trends (10^{13} molecules per cm^2 per year)
	-1.99 ± 0.04				Relative trends (% per year)

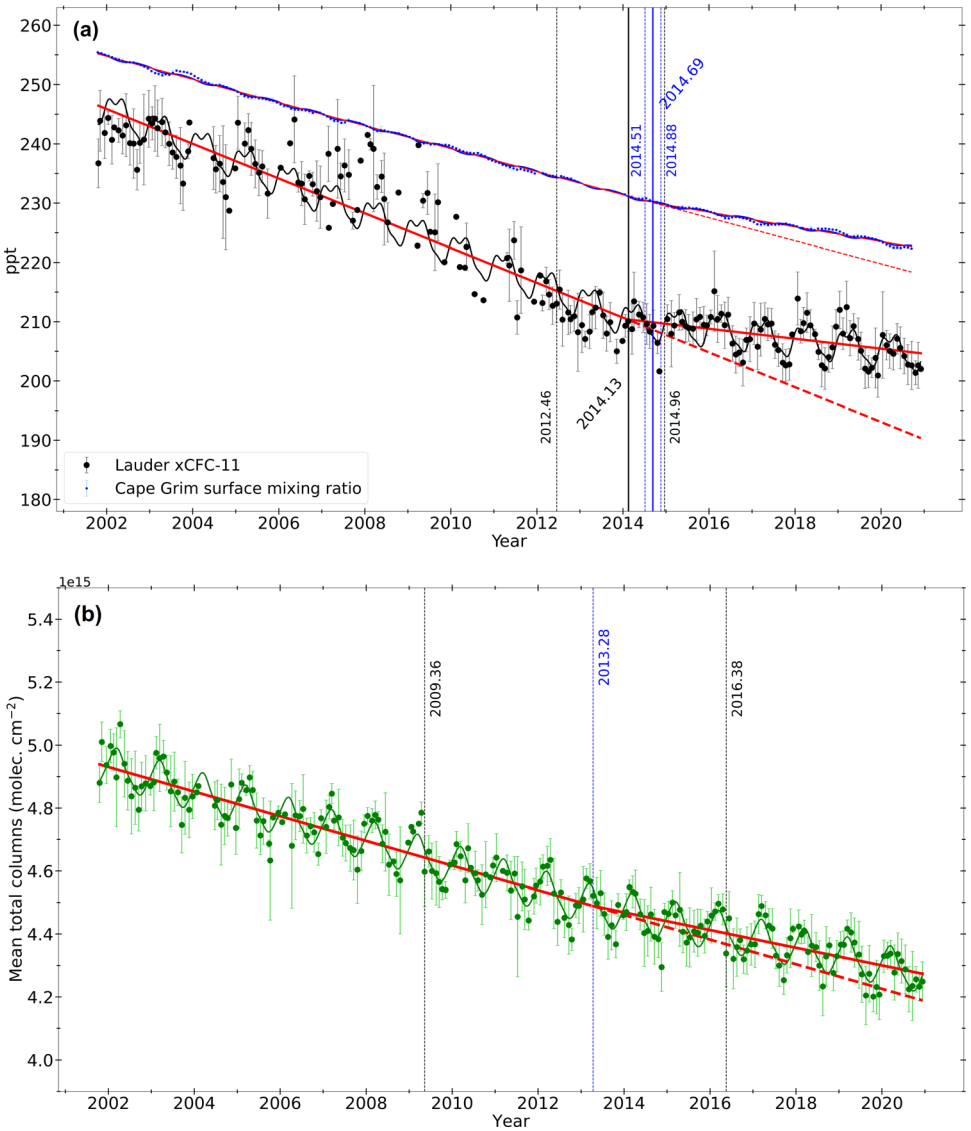

Fig. 6 (a) *In situ* monthly CFC-11 at Cape Grim (in blue) and monthly xCFC-11 FTIR above Lauder (in black). (b) TOMCAT model monthly time series of CFC-11 total columns above Lauder. The "best estimation/realistic" simulation (tracer A) has been chosen. All vertical bars represent the standard deviations around the monthly means.

found for the observations fits inside the confidence interval of the model data break location.

The trends before and after the break points, as well as the long-term trends (2001–2020) for the Cape Grim and Lauder stations, and for the model results for Lauder are listed in Table 3. Note that model trends are shown in total columns (molecules per cm^2 per year), while *in situ* Cape Grim trends and FTIR Lauder trends are displayed in ppt per year. We computed the xCFC-11 trends (LAU) without the unexpectedly high points between 2007 and 2009.5 in order to verify if the trends values changed. The relative trend before the break point obtained is (-1.34 ± 0.08)% per year, while the trend after the break point is (-0.33 ± 0.10)% per year. The break location estimated without the 2007–2009.5 data is $2013.81^{+0.71}_{-1.14}$. As it can be observed, the trends values and the break location (with and without this period) did not change significantly. The results presented in Table 3 are those obtained for the whole dataset.

For the Cape Grim *in situ* observations, the pre-break trend decreases by (0.82 ± 0.01)% per year, while the post-break trend decay is (0.52 ± 0.01)% per year, which is a 58% change in the trend. For the model simulations for the Lauder location, the trend before the break is (-0.86 ± 0.05)% per year, while the trend after the break is (-0.61 ± 0.07)% per year, bringing about a 41% trend change. For the Lauder xCFC-11 series, the pre-break trend is (-1.34 ± 0.08)% per year, while the post-break trend is (-0.39 ± 0.10)% per year, which is near in the limit of the confidence interval of the other two time series' post-break trends.

A significant point to note is the agreement between the relative trends. As one can observe, the relative trend for the whole time series (2001–2020) is the same for Cape Grim and for

Table 3 CFC-11 annual trends derived from the *in situ* measurements at Cape Grim, xCFC-11 and CFC-11 annual trends derived from the Lauder FTIR time series and TOMCAT model

	2001–2020	Break location	2001 to Break	Break to 2020	
In situ Cape Grim	−1.77 ± 0.02	2014.69	−1.94 ± 0.01	−1.23 ± 0.03	Surface mixing ratio trends (ppt per year)
	−0.74 ± 0.01		−0.82 ± 0.01	−0.52 ± 0.01	Relative trends (% per year)
xCFC-11 FTIR LAU	−2.32 ± 0.08	2014.13	−2.94 ± 0.17	−0.86 ± 0.23	Dry air mole fraction trends (ppt per year)
	−1.05 ± 0.04		−1.34 ± 0.08	−0.39 ± 0.10	Relative trends (% per year)
xCFC-11 TOMCAT for LAU (tracer A run)	−1.72 ± 0.05	2011.25	−2.05 ± 0.15	−1.38 ± 0.12	Dry air mole fraction trends (ppt per year)
	−0.77 ± 0.02		−0.92 ± 0.06	−0.62 ± 0.05	Relative trends (% per year)
TOMCAT for LAU (tracer A run)	−3.52 ± 0.11	2013.28	−3.92 ± 0.22	−2.81 ± 0.33	Total columns trends (10^{13} molecules per cm^2 per year)
	−0.77 ± 0.02		−0.86 ± 0.05	−0.61 ± 0.07	Relative trends (% per year)
xCFC-11 TOMCAT for LAU (tracer C run)	−3.86 ± 0.05	—	—	—	Dry air mole fraction trends (ppt per year)
	−1.96 ± 0.03				Relative trends (% per year)
TOMCAT for LAU (tracer C run)	−7.93 ± 0.10	—	—	—	Total columns trends (10^{13} molecules per cm^2 per year)
	−1.96 ± 0.02				Relative trends (% per year)

the model and quite close for Lauder (36% difference), considering the unexplained feature of this time series. Regarding the pre-break and post-break relative trends, this behaviour is the same.

4.3.3 Inter-hemispheric analysis. In the case of the Jungfraujoch site, all the trends (long-term, pre-break, and post-break) are in a very good agreement (*i.e.* within uncertainty estimates). For the Lauder site, there were some differences because of the unexpectedly high data over 2007–2009.5. Through the comparison with the Cape Grim *in situ* observations, we can see that the relative trends between the observations and the model are also in good agreement. Regarding the long-term trends (2000–2020), they are quite similar in both hemispheres, both for the model and the observations. Before the break point, the trend decay in the NH was more important than in the SH (10% larger for the observations and 20% larger for the model simulations). The post-break trend decrease is 27% larger in the NH for the observations, while it is 10% smaller for the model results than in the SH. Nevertheless, if we take into account the errors of each trend, we can affirm that all of the trend values lie within the error limits (see Tables 2 and 3).

The Report on the Unexpected Emissions of CFC-11, 2021 [4] documents that the CFC-11 atmospheric global concentrations decayed by 0.8% per year from 2002 to 2012, and by 0.5% per year from 2014 to 2018. Fortunately, the atmospheric concentrations declined faster between 2018 and 2019 (by 0.7% per year). If we compare these trends to our observations, we can affirm that they are in a very good agreement. For the pre-break period, we obtained a decay of (0.95 ± 0.13)% per year (2000–2011) in the NH, and a decay of (0.82 ± 0.01)% per year (2001–2014) in the SH (Cape Grim). For the post-break period, we obtained a decay of (0.61 ± 0.15)% per year (2011–2020) in the NH. In the SH, we got a decay of (0.52 ± 0.01)% per year for Cape Grim, and (0.39 ± 0.10)% per year for Lauder (2014–2020). Nevertheless, nowadays we cannot detect trend changes like the one after 2018 with FTIR observations, even for daily averages. We will need a longer time series after 2018 to be able to detect it.

According to Holzer and Waugh, 2015,[46] the tropospheric mean time needed for the CFCs to travel from the NH, where the principal emissions happen, to the SH varies from 1.1 years (in the South Hemisphere tropics) to 1.4 years (at the South Pole). These values are compatible with our observations and TOMCAT simulations, taking into account the uncertainty ranges.

5. Conclusions

We have applied consistent retrievals and analysed CFC-11 total column time series, using Jungfraujoch and Lauder high-resolution FTIR solar spectra recorded within the framework of the NDACC network. For the first time, the Jungfraujoch time series was extended back to include spectra recorded before the 2000s, and fully harmonised to account for instrument replacements and upgrades. Our study is the first to present a merged CFC-11 FTIR dataset from Lauder. In both cases, we adopted a large spectral window (830.0–859.3 cm^{-1}) so as to include the broad CFC-11 feature, accounting for the interfering species, notably water vapour. The DOFS values are 1.36 for Jungfraujoch, and 1.57 for Lauder. The estimates of the relative total random and systematic uncertainties are 3.3% and 7.5%, respectively, for the Jungfraujoch station, and 2.2% and 7.2%, respectively, for the Lauder station.

The FTIR time series, supplemented with *in situ* surface data from Cape Grim, were compared with a TOMCAT model run implementing the undeclared CFC-11 emissions reported by Montzka *et al.*, 2018,[7] quantitatively confirming their impact on atmospheric CFC-11, both on the vertical and horizontal scales.

Trends between 2000 and 2020 were analysed for the Jungfraujoch station and between 2001 and 2020 for the Lauder and Cape Grim stations. Very good agreement was found between the observations and the model trends, especially for the Jungfraujoch station. A break point around 2011 was found for the Jungfraujoch FTIR and model data, while it appears around 2014 for the Southern Hemisphere. In the Northern Hemisphere, total columns declined by (0.95 ± 0.13)% per year and (1.03 ± 0.08)% per year (between 2000 and 2011), for the FTIR

and model time series, respectively. A slowdown in the decay was observed after 2011, where we obtained a decay of (0.61 ± 0.15)% per year and (0.55 ± 0.09)% per year (between 2011 and 2020), for the FTIR and model time series respectively. In the Southern Hemisphere, the relative trends before the break point (2001–2014) are (−0.82 ± 0.01)% per year and (−0.86 ± 0.05)% per year, for the *in situ* and model datasets, respectively; while the relative trends after the break point (2014–2020) are (−0.52 ± 0.01)% per year, (−0.39 ± 0.10)% per year, and (−0.61 ± 0.07)% per year, for the *in situ*, FTIR, and model time series, respectively. These values are in a good agreement with those reported by the Report on the Unexpected Emissions of CFC-11, 2021.[4] Therefore, the trend decrease slowdown after the break point was around 56% for the Jungfraujoch CFC-11 total columns and around 58% for the Cape Grim *in situ* observations.

These trend changes confirm that FTIR measurements are able to detect variations in CFC-11 emissions of the order of magnitude of those reported by Rigby *et al.*, 2019.[8] Taking into account the uncertainties, the differences in the break location between the Northern (≈2011) and the Southern (≈2014) Hemispheres are representative of the mean interhemispheric transit time, estimated as ≈1.1 years in the Southern Hemisphere tropics, and ≈1.4 years at the South Pole by Holzer and Waugh, 2015.[46]

Our results confirm the success of the Montreal Protocol which has been able to significantly reduce CFC-11 emissions. Still, renewed emissions related to illegal production occurred for a few years but were quickly identified[7,8] and appear to have now decreased significantly.[11,12] These FTIR measurements can also be used to monitor CFC-11 and help to detect rogue emissions, of a magnitude similar to that observed in 2012–2018, providing complementary monitoring to surface-measurement networks.

Because of the constant monitoring of the atmosphere, the scientific community has been able to swiftly spot non-compliant emissions of CFC-11 and identify their origin, which apparently led to their reduction. It is important to note that the model simulations implementing these additional emissions, the surface *in situ* and ground-based remote sensing time series, together provide a very consistent picture demonstrating a proper understanding of the processes driving the CFC-11 atmospheric burden and its evolution.

Data availability

The Jungfraujoch and Lauder FTIR data are available upon request (i.pardocantos@uliege.be and dan.smale@niwa.co.nz, respectively). The *in situ* Cape Grim data are available at the Advanced Global Atmospheric Gases Experiment (AGAGE) website (**https://agage2.eas.gatech.edu/data_archive/agage/gc-md/complete/tasmania/**). ACE data are available at the ACE/SCISAT Database (**https://databace.scisat.ca/level2/**). MIPAS version 8 CFC-11 data were retrieved with the IMK/IAA research processor and provided by **https://www.imk-asf.kit.edu/english/308.php**.

Author contributions

IPC: conceptualization, data curation, formal analysis, investigation, methodology, software, visualization, writing – original draft. EM: conceptualization, data curation, funding acquisition, investigation, methodology and supervision. MPC: data curation, writing. DS: data curation, writing. JWH: methodology. MF: software. PF: data curation, writing. PK: data curation, writing. MP: software. JM: data curation. CS: spectra acquisition, instruments maintenance and development. JR: spectra acquisition and data curation.

Conflicts of interest

There are no conflicts to declare.

Acknowledgements

This work has been supported by the Fonds de la Recherche Scientifique (F.R.S. – FNRS, Brussels, Belgium; grant no. J.0126.21), the GAW-CH program of MeteoSwiss (Zürich, CH) and the University of Liège. EM is a senior research associate with F.R.S. – FNRS. The ULiège team thanks the International Foundation High Altitude Research Stations Jungfraujoch and Gornergrat (HFSJG, Bern, CH) for supporting the facilities needed to perform the Fourier transform infrared observations at Jungfraujoch. The FTIR measurements made at Lauder are core-funded by NIWA through New Zealand's Ministry of Business, Innovation and Employment Strategic Science Investment Fund. MPC was supported by the UK Natural Environment Research Council SISLAC project (NE/R001782/1). The TOMCAT model runs were performed on the UK Archer and University of Leeds ARC computers. The AGAGE operation at Cape Grim is funded by the Bureau of Meteorology, CSIRO Oceans and Atmosphere and MIT (NASA). The National Center for Atmospheric Research is sponsored by the National Science Foundation. We thank Dr G. C. Toon for developing, maintaining and making available the pseudolinelists (PLLs) and the ATM2019 spectroscopic compilation that were essential to the present work. The Atmospheric Chemistry Experiment (ACE) is funded by the Canadian Space Agency.

References

1 E. L. Fleming, P. A. Newman, Q. Liang and J. S. Daniel, The impact of continuing CFC-11 emissions on stratospheric ozone, *J. Geophys. Res.: Atmos.*, 2020, **125**(3), DOI: **10.1029/2019JD031849**.

2 M. J. Molina and F. S. Rowland, Stratospheric sink for chlorofluoromethanes: chlorine atom-catalysed destruction of ozone, *Nature*, 1974, **249**, 810–812, DOI: **10.1038/249810a0**.

3 J. C. Farman, B. G. Gardinier and J. D. Shanklin, Large losses of total ozone in Antarctica reveal seasonal ClOx/NOx interaction, *Nature*, 1985, **315**, 207–210, DOI: **10.1038/315207a0**.

4 M. Chipperfield, M. Hegglin, S. Montzka, P. Newman, S. Park, S. Reimann, M. Rigby, A. Stohl, G. Velders, H. Walter-Terrinoni *et al.*, *Report on Unexpected Emissions of CFC-11*, World Meteorological Organization (WMO) Technical Report, 2021.

5 M. Lickley, S. Solomon, S. Fletcher, G. J. Velders, J. Daniel, M. Rigby, S. A. Montzka, L. J. Kuijpers and K. Stone, Quantifying contributions of chlorofluorocarbon banks to emissions and impacts on the ozone layer and climate, *Nat. Commun.*, 2020, **11**, 1–11, DOI: **10.1038/s41467-020-15162-7**.

6 WMO, *Scientific assessment of ozone depletion: 2018, global ozone research and monitoring project, Report No. 58*, 2018.

7 S. A. Montzka, G. S. Dutton, P. Yu, E. Ray, R. W. Portmann, J. S. Daniel, L. Kuijpers, B. D. Hall, D. Mondeel, C. Siso, J. D. Nance, M. Rigby, A. J. Manning, L. Hu, F. Moore, B. R. Miller and J. W. Elkins, An unexpected and persistent increase in global emissions of ozone-depleting CFC-11, *Nature*, 2018, **557**, 413–417, DOI: **10.1038/s41586-018-0106-2**.

8 M. Rigby, S. Park, T. Saito, L. M. Western, A. L. Redington, X. Fang, S. Henne, A. J. Manning, R. G. Prinn, G. S. Dutton, P. J. Fraser, A. L. Ganesan, B. D. Hall, C. M. Harth, J. Kim, J.-R. Kim, P. B. Krummel, T. Lee, S. Li, Q. Liang, M. F. Lunt, S. A. Montzka, J. Mühle, S. O'Doherty, M.-K. Park, S. Reimann, P. K. Salameh, P. Simmonds, R. L. Tunnicliffe, R. F. Weiss, Y. Yokouchi and D. Young, Increase in CFC-11 emissions from eastern China based on atmospheric observations, *Nature*, 2019, **569**, 546–550, DOI: **10.1038/s41586-019-1193-4**.

9 P. F. Bernath, J. Steffen, J. Crouse and C. D. Boone, Sixteen-year trends in atmospheric trace gases from orbit, *J. Quant. Spectrosc. Radiat. Transfer*, 2020, **253**, 107–178, DOI: **10.1016/j.jqsrt.2020.107178**.

10 S. Dhomse, W. Feng, S. A. Montzka, R. Hossaini, J. Keeble, J. Pyle, J. Daniel and M. Chipperfield, Delay in recovery of the Antarctic ozone hole from unexpected CFC-11 emissions, *Nat. Commun.*, 2019, **10**, 1–12, DOI: **10.1038/s41467-019-13717-x**.

11 S. A. Montzka, G. S. Dutton, R. W. Portmann, M. P. Chipperfield, S. Davis, W. Feng, A. J. Manning, E. Ray, M. Rigby, B. D. Hall, C. Siso, J. D. Nance, P. B. Krummel, J. Mühle, D. Young, S. O'Doherty, P. K. Salameh, C. M. Harth, R. G. Prinn, R. F. Weiss, J. W. Elkins, H. Walter-Terrinoni and C. Theodoridi, A decline in global CFC-11 emissions during 2018–2019, *Nature*, 2021, 1–5, DOI: **10.1038/s41586-021-03260-5**.

12 S. Park, L. M. Western, T. Saito, A. L. Redington, S. Henne, X. Fang, R. G. Prinn, A. J. Manning, S. A. Montzka, P. J. Fraser, A. L. Ganesan, C. M. Harth, J. Kim, P. B. Krummel, Q. Liang, J. Mühle, S. O'Doherty, H. Park, M.-K. Park, S. Reimann, P. K. Salameh, R. F. Weiss and M. Rigby, A decline in emissions of CFC-11 and related chemicals from eastern China, *Nature*, 2021, 1–5, DOI: **10.1038/s41586-021-03277-w**.

13 M. De Mazière, A. M. Thompson, M. J. Kurylo, J. D. Wild, G. Bernhard, T. Blumenstock, G. O. Braathen, J. W. Hannigan, J.-C. Lambert, T. Leblanc, T. J. McGee, G. Nedoluha, I. Petropavlovskikh, G. Seckmeyer, P. C. Simon, W. Steinbrecht and S. E. Strahan, The Network for the Detection of Atmospheric Composition Change (NDACC): history, status and perspectives, *Atmos. Chem. Phys.*, 2018, **18**, 4935–4964, DOI: **10.5194/acp-18-4935-2018**.

14 R. G. Prinn, R. F. Weiss, J. Arduini, T. Arnold, H. L. DeWitt, P. J. Fraser, A. L. Ganesan, J. Gasore, C. M. Harth, O. Hermansen, J. Kim, P. B. Krummel, S. Li, Z. M. Loh, C. R. Lunder, M. Maione, A. J. Manning, B. R. Miller, B. Mitrevski, J. Mühle, S. O'Doherty, S. Park, S. Reimann, M. Rigby, T. Saito, P. K. Salahem, R. Schmidt, P. G. Simmonds, L. P. Steele, M. K. Vollmer, R. H. Wang, B. Yao, Y. Yokouchi, D. Young and L. Zhou, History of chemically and radiatively important atmospheric gases from the Advanced Global Atmospheric Gases Experiment (AGAGE), *Earth Syst. Sci. Data*, 2018, **10**, 985–1018, DOI: **10.5194/essd-10-985-2018**.

15 M. Prignon, S. Chabrillat, D. Minganti, S. O'Doherty, C. Servais, G. Stiller, G. C. Toon, M. K. Vollmer and E. Mahieu, Improved FTIR retrieval strategy for HCFC-22 ($CHClF_2$), comparisons with in situ and satellite datasets with the support of models, and determination of its long-term trend above Jungfraujoch, *Atmos. Chem. Phys.*, 2019, **19**, 12309–12324, DOI: **10.5194/acp-19-12309-2019**.

16 R. Zander, E. Mahieu, P. Demoulin, P. Duchatelet, G. Roland, C. Servais, M. De Mazière, S. Reimann and C. P. Rinsland, Our changing atmosphere: Evidence based on long-term infrared solar observations at the Jungfraujoch since 1950, *Sci. Total Environ.*, 2008, **391**, 184–195, DOI: **10.1016/j.scitotenv.2007.10.018**.

17 J. Robinson, D. Smale, D. Pollard and H. Shiona, Solar tracker with optical feedback and continuous rotation, *Atmos. Meas. Tech.*, 2020, **13**, 5855–5871, DOI: **10.5194/amt-13-5855-2020**.

18 C. Vigouroux, T. Blumenstock, M. Coffey, Q. Errera, O. García, N. B. Jones, J. Hannigan, F. Hase, B. Liley, E. Mahieu, J. Mellqvist, J. Notholt, M. Palm, G. Persson, M. Schneider, C. Servais, D. Smale, L. Thölix and M. De Mazière, Trends of ozone total columns and vertical distribution from FTIR observations at eight NDACC stations around the globe., *Atmos. Chem. Phys.*, 2015, **15**, 2915–2933, DOI: **10.5194/acp-15-2915-2015**.

19 G. Ronsmans, B. Langerock, C. Wespes, J. W. Hannigan, F. Hase, T. Kerzenmacher, E. Mahieu, M. Schneider, D. Smale, D. Hurtmans, M. De Mazière, C. Clerbaux and P.-F. Coheur, First characterization and validation of FORLI-HNO_3 vertical profiles retrieved from IASI/Metop, *Atmos. Meas. Tech.*, 2016, **9**, 4783–4801, DOI: **10.5194/amt-9-4783-2016**.

20 R. Kohlhepp, R. Ruhnke, M. P. Chipperfield, M. De Mazière, J. Notholt, S. Barthlott, R. L. Batchelor, R. D. Blatherwick, T. Blumenstock, M. Coffey, P. Demoulin, H. Fast, W. Feng, A. Goldman, D. W. T. Griffith, K. Hamann, J. W. Hannigan, F. Hase, N. B. Jones, A. Kagawa, I. Kaiser, Y. Kasai, O. Kirner, W. Kouker, R. Lindenmaier, E. Mahieu, R. L. Mittermeier, B. Monge-Sanz, I. Morino, I. Murata,

H. Nakajima, M. Palm, C. Paton-Walsh, U. Raffalski, Th. Reddmann, M. Rettinger, C. P. Rinsland, E. Rozanov, M. Schneider, C. Senten, C. Servais, B.-M. Sinnhuber, D. Smale, K. Strong, R. Sussmann, J. R. Taylor, G. Vanhaelewyn, T. Warneke, C. Whaley, M. Wiehle and S. W. Wood, Observed and simulated time evolution of HCl, $ClONO_2$, and HF total column abundances, *Atmos. Chem. Phys.*, 2012, **12**, 3527–3556, DOI: **10.5194/acp-12-3527-2012**.

21 F. Hase, T. Blumenstock and C. Paton-Walsh, Analysis of the instrumental line shape of high-resolution Fourier transform IR spectrometers with gas cell measurements and new retrieval software, *Appl. Opt.*, 1999, **38**, 3417–3422, DOI: **10.1364/AO.38.003417**.

22 F. Hase, Improved instrumental line shape monitoring for the ground-based, high-resolution FTIR spectrometers of the Network for the Detection of Atmospheric Composition Change, *Atmos. Meas. Tech.*, 2012, **5**, 603–610, DOI: **10.5194/amt-5-603-2012**.

23 P. Fraser, P. Hyson, I. Enting and G. Pearman, Global distribution and southern hemispheric trends of atmospheric CCl_3F, *Nature*, 1983, **302**, 692–695, DOI: **10.1038/302692a0**.

24 P. J. Fraser, G. I. Pearman and N. Derek, CSIRO Non-carbon dioxide greenhouse gas research. Part 1: 1975–90, *Hist. Rec. Aust. Sci.*, 2018, **29**, 1–13, DOI: **10.1071/HR17016**.

25 M. Chipperfield, New version of the TOMCAT/SLIMCAT off-line chemical transport model: Intercomparison of stratospheric tracer experiments, *Q. J. R. Metereol. Soc.*, 2006, **132**, 1179–1203, DOI: **10.1256/qj.05.51**.

26 H. Hersbach, B. Bell, P. Berrisford, S. Hirahara, A. Horányi, J. Muñoz-Sabater, J. Nicolas, C. Peubey, R. Radu, D. Schepers, A. Simmons, C. Soci, S. Abdalla, X. Abellan, G. Balsamo, P. Bechtold, G. Biavati, J. Bidlot, M. Bonavita, G. De Chiara, P. Dahlgren, D. Dee, M. Diamantakis, R. Dragani, J. Flemming, R. Forbes, M. Fuentes, A. Geer, L. Haimberger, S. Healy, R. J. Hogan, E. Hólm, M. Janisková, S. Keeley, P. Laloyaux, P. Lopez, C. Lupu, G. Rednoti, P. de Rosnay, I. Rozum, F. Vamborg, S. Villaume and J.-N. Thépaut, The ERA5 global reanalysis, *Q. J. R. Metereol. Soc.*, 2020, **146**, 1999–2049, DOI: **10.1002/qj.3803**.

27 M. Tiedtke, A comprehensive mass flux scheme for cumulus parameterization in large-scale models, *Mon. Weather Rev.*, 1989, **117**, 1779–1800, DOI: **10.1175/1520-0493(1989)117<1779:ACMFSF>2.0.CO;2**.

28 A. Holtslag and B. Boville, Local versus nonlocal boundary-layer diffusion in a global climate model, *J. Clim.*, 1993, **6**, 1825–1842, DOI: **10.1175/1520-0442(1993)006<1825:LVNBLD>2.0.CO;2**.

29 C. D. Rodgers, *Inverse Methods for Atmospheric Sounding: Theory and Practice*, World Scientific, 2000, vol. 2.

30 R. Zander, G. M. Stokes and J. W. Brault, Simultaneous detection of FC-11, FC-12 and FC-22, through 8 to 13 Micrometers IR solar observations from the ground, *Geophys. Res. Lett.*, 1983, **10**, 521–524, DOI: **10.1029/GL010i007p00521**.

31 L. S. Rothman, I. E. Gordon, A. Barbe, D. C. Benner, P. F. Bernath, M. Birk, V. Boudon, L. R. Brown, A. Campargue, J.-P. Champion, K. Chance, L.-H. Coudert, V. Dana, V. M. Devi, S. Fally, J.-M. Flaud, R. R. Gamache, A. Goldman, D. Jacquemart, I. Kleiner, N. Lacome, W. J. Lafferty, J.-Y. Mandin, S. T. Massie, S. N. Mikhailenko, C. E. Miller, N. Moazzen-Ahmadi, O. V. Naumenko, A. V. Nikitin, J. Orphal, V. I. Perevalov, A. Perrin, A. Predoi-Cross, C. P. Rinsland, M. Rotger, M. Šimečková, M. A. H. Smith, K. Sung, S. A. Tashkun, J. Tennyson, R. A. Toth, A. C. Vandaele and J. Vander Auwera, The HITRAN 2008 molecular spectroscopic database, *J. Quant. Spectrosc. Radiat. Transfer*, 2009, **110**, 533–572, DOI: **10.1016/j.jqsrt.2009.02.013**.

32 L. S. Rothman, I. E. Gordon, Y. Babikov, A. Barbe, D. C. Benner, P. F. Bernath, M. Birk, L. Bizzocchi, V. Boudon, L. R. Brown, A. Campargue, K. Chance, E. A. Cohen, L. H. Coudert, V. M. Devi, B. J. Drouin, A. Fayt, J.-M. Flaud, R. R. Gamache, J. J. Harrison, J.-M. Hartmann, C. Hill, J. T. Hodges, D. Jacquemart, A. Jolly, J. Lamouroux, R. J. Le Roy, G. Li, D. A. Long, O. M. Lyulin, C. J. Mackie, S. T. Massie, S. Mikhailenko, H. S. P. Müller, O. V. Naumenko, A. V. Nikitin, J. Orphal, V. Perevalov, A. Perrin, E. R. Polovtseva, C. Richard, M. A. H. Smith, E. Starikova, K. Sung, S. Tashkun, J. Tennyson, G. C. Toon, Vl. G. Tyuterev and G. Wagner, The HITRAN2012 molecular spectroscopic database, *J. Quant. Spectrosc. Radiat. Transfer*, 2013, **130**, 4–50, DOI: **10.1016/j.jqsrt.2013.07.002**.

33 F. Hase, P. Demoulin, A. Sauval, G. Toon, P. Bernath, A. Goldman, J. Hannigan and C. Rinsland, An empirical line-by-line model for the infrared solar transmittance spectrum from 700 to 5000 cm^{-1}, *J. Quant. Spectrosc. Radiat. Transfer*, 2006, **102**, 450–463, DOI: **10.1016/j.jqsrt.2006.02.026**.

34 D. R. Marsh, M. J. Mills, D. E. Kinnison, J.-F. Lamarque, N. Calvo and L. M. Polvani, Climate change from 1850 to 2005 simulated in CESM1 (WACCM), *J. Clim.*, 2013, **26**, 7372–7391, DOI: **10.1175/JCLI-D-12-00558.1**.

35 P. Berrisford, D. Dee, P. Poli, R. Brugge, K. Fielding, M. Fuentes, P. Kållberg, S. Kobayashi, S. Uppala and A. Simmons, 2011, *The ERA-Interim archive Version 2.0*, 2011, p. 1.

36 E. Kalnay, M. Kanamitsu, R. Kistler, W. Collins, D. Deaven, L. Gandin, M. Iredell, S. Saha, G. White, J. Woollen, Y. Zhu, M. Chelliah, W. Ebisuzaki, W. Higgins, J. Janowiak, K. C. Mo, C. Ropelewski, J. Wang, A. Leetmaa, R. Reynolds, R. Jenne and D. Joseph, The NCEP/NCAR 40-Year Reanalysis Project, *Bull. Am. Meteorol. Soc.*, 1996, **77**, 437–472, DOI: **10.1175/1520-0477(1996)077<0437:TNYRP>2.0.CO;2**.

37 M. Zhou, C. Vigouroux, B. Langerock, P. Wang, G. Dutton, C. Hermans, N. Kumps, J.-M. Metzger, G. Toon and M. De Mazière, CFC-11, CFC-12 and HCFC-22 ground-based remote sensing FTIR measurements at Réunion Island and comparisons with MIPAS/ENVISAT data, *Atmos. Meas. Tech.*, 2016, **9**, 5621–5636, DOI: **10.5194/amt-9-5621-2016**.

38 C. Boone, S. Jones and P. Bernath, *Data Usage Guide and File Format Description for ACE-FTS Level 2 Data Version 4.0 ASCII Format*, 2019, **https://g-624536.53220.5898.data.globus.org/1/published/publication_286/submitted_data/ACE-SOC-0033-ACE-FTS_ascii_data_usage_and_fileformat_for_v4.0.pdf**.

39 B. M. Dinelli, P. Raspollini, M. Gai, L. Sgheri, M. Ridolfi, S. Ceccherini, F. Barbara, N. Zoppetti, E. Castelli, E. Papandrea, P. Pettinari, A. Dehn, A. Dudhia, M. Kiefer, A. Piro, J.-M. Flaud, M. López-Puertas, D. Moore, J. Remedios and M. Bianchini, The ESA MIPAS/Envisat level2-v8 dataset: 10 years of measurements retrieved with ORM v8.22, *Atmos. Meas. Tech.*, 2021, **14**, 7975–7998, DOI: **10.5270/EN1-c8hgqx4**.

40 A. Polyakov, A. Poberovsky, M. Makarova, Y. Virolainen, Y. Timofeyev and A. Nikulina, Measurements of CFC-11, CFC-12, and HCFC-22 total columns in the atmosphere at the St. Petersburg site in 2009–2019, *Atmos. Meas. Tech.*, 2021, **14**, 5349–5368, DOI: **10.5194/amt-14-5349-2021**.

41 E. Mahieu, E. V. Fischer, B. Franco, M. Palm, T. Wizenberg, D. Smale, L. Clarisse, C. Clerbaux, P.-F. Coheur, J. W. Hannigan, E. Lutsch, J. Notholt, I. Pardo Cantos, M. Prignon, C. Servais and K. Strong, First retrievals of peroxyacetyl nitrate (PAN) from ground-based FTIR solar spectra recorded at remote sites, comparison with model and satellite data, *Elem Sci Anth*, 2021, **9**, 00027, DOI: **10.1525/elementa.2021.00027**.

42 M. Friedrich, S. Smeekes and J.-P. Urbain, Autoregressive wild bootstrap inference for nonparametric trends, *J. Econom.*, 2020, **214**, 81–109, DOI: **10.1016/j.jeconom.2019.05.006**.

43 M. Friedrich, E. Beutner, H. Reuvers, S. Smeekes, J.-P. Urbain, W. Bader, B. Franco, B. Lejeune and E. Mahieu, A statistical analysis of time trends in atmospheric ethane, *Clim. Change*, 2020, **162**, 105–125, DOI: **10.1007/s10584-020-02806-2**.

44 S. Barthlott, M. Schneider, F. Hase, A. Wiegele, E. Christner, Y. González, T. Blumenstock, S. Dohe, O. García, E. Sepúlveda, K. Strong, J. Mendonca, D. Weaver, M. Palm, N. M. Deutscher, T. Warneke, J. Notholt, B. Lejeune, E. Mahieu, N. Jones, D. W. T. Griffith, V. A. Velazco, D. Smale, J. Robinson, R. Kivi, P. Heikkinen and U. Raffalski, Using XCO_2 retrievals for assessing the long-term consistency of NDACC/FTIR data sets, *Atmos. Meas. Tech.*, 2015, **8**, 1555–1573, DOI: **10.5194/amt-8-1555-2015**.

45 J. L. Bullister, Atmospheric Histories (1765-2015) for CFC-11, CFC-12, CFC-113, CCl_4, SF_6 and N_2O (NCEI Accession 0164584), *NOAA National Centers for Environmental Information*, 2017, Unpublished Dataset, DOI: **10.3334/CDIAC/otg.CFC_ATM_Hist_2015**.

46 M. Holzer and D. W. Waugh, Interhemispheric transit time distributions and path-dependent lifetimes constrained by measurements of SF_6, CFCs, and CFC replacements, *Geophys. Res. Lett.*, 2015, **42**, 4581–4589, DOI: **10.1002/2015GL064172**.